

Demonstration of 4.8×10^{-17} stability at 1 s for two independent optical clocks

E. Oelker^{1*}, R. B. Hutson¹, C. J. Kennedy¹, L. Sonderhouse¹, T. Bothwell¹, A. Goban¹, D. Kedar¹, C. Sanner¹, J. M. Robinson¹, G. E. Marti^{1,5}, D. G. Matei^{2,6}, T. Legero^{1,7}, M. Giunta^{1,3,4}, R. Holzwarth^{3,4}, F. Riehle², U. Sterr^{1,7} and J. Ye^{1*}

Optical atomic clocks require local oscillators with exceptional optical coherence owing to the challenge of performing spectroscopy on their ultranarrow-linewidth clock transitions. Advances in laser stabilization have thus enabled rapid progress in clock precision. A new class of ultrastable lasers based on cryogenic silicon reference cavities has recently demonstrated the longest optical coherence times to date. Here we utilize such a local oscillator with two strontium (Sr) optical lattice clocks to achieve an advance in clock stability. Through an anti-synchronous comparison, the fractional instability of both clocks is assessed to be $4.8 \times 10^{-17}/\sqrt{\tau}$ for an averaging time τ (in seconds). Synchronous interrogation enables each clock to average at a rate of $3.5 \times 10^{-17}/\sqrt{\tau}$, dominated by quantum projection noise, and reach an instability of 6.6×10^{-19} over an hour-long measurement. The ability to resolve sub- 10^{-18} -level frequency shifts in such short timescales will affect a wide range of applications for clocks in quantum sensing and fundamental physics.

Atomic frequency standards play a vital part in a growing number of technological and scientific endeavours. Atomic clocks based on microwave transitions currently define the SI (the International System of Units) second and are used extensively for network synchronization and satellite-based navigation systems such as the Global Positioning System (GPS). Over the past two decades, a new generation of atomic clocks based on narrow-linewidth optical transitions has reached maturity and now surpasses its microwave predecessors in both accuracy and stability^{1–6}. Further improvements in clock performance will help pave the way for the eventual redefinition of the SI second in terms of an optical transition⁷. Optical clocks are also ideal for observing physical phenomena that cause minute alterations in the clock transition frequency. They can be used to detect possible drift in the values of fundamental constants^{8–10}, enable relativistic geodesy^{6,11,12}, test fundamental symmetries^{13,14} and even potentially detect passing gravitational waves¹⁵ or dark matter^{16,17}.

All of these exciting applications have one thing in common: they require ultrastable frequency comparison measurements between two or more atomic clocks. The stability is a measure of the noise of a frequency standard and is often expressed as fractional frequency fluctuations $\delta\nu_c/\nu_c$ where ν_c is the clock transition frequency. Quantum projection noise (QPN) determines the standard quantum limit (SQL) for the clock instability¹⁸. For Rabi spectroscopy, this limit is given by

$$\sigma_{\text{QPN}}(\tau) = \frac{0.264}{\nu_c T_p} \sqrt{\frac{T_c}{N\tau}} \quad (1)$$

where T_p is the Rabi spectroscopy time, T_c is the clock cycle time and N is the number of atoms.

In neutral atom optical lattice clocks, thousands of atoms are interrogated simultaneously, leading to a favourably small SQL for

clock instability. However, optical lattice clocks generally operate with an instability above this limit due to noise on the laser used to probe the clock transition. The clock transition typically cannot be measured continuously, as time is required for sample preparation and state detection. During the interval between successive measurements, hereafter referred to as dead time, the local oscillator serves as a flywheel and largely determines the stability of the clock. Owing to the intermittency of the measurements, high-frequency noise from the probe laser is aliased down to lower frequencies, degrading the clock stability at long averaging times. So far, this technical noise coupling, known as the Dick effect, has limited single-ensemble instability^{1,4,19–21} to the low $10^{-16}/\sqrt{\tau}$ level. Advances in the stability of local oscillators will improve optical clock performance by reducing the Dick effect and enabling longer interrogation times, leading to enhanced spectroscopic resolution²² and a lower QPN bound. Progress in laser stabilization has also facilitated studies of spin-orbit coupling²³ and many-body physics^{24,25}.

Recently, conventional optical local oscillators referenced to ultralow-expansion (ULE) glass cavities have reached the performance bound set by fundamental thermo-mechanical noise from their constituent materials^{26,27}. To reach a new stability regime, we have developed an improved class of ultrastable lasers based on cryogenic silicon reference cavities^{28–31}. The local oscillator used in this work is referenced to a 21 cm silicon (Si) cavity operating at 124 K. Its performance was evaluated by comparing two identical systems²⁹, each exhibiting a sub-10 mHz linewidth, a laser coherence time of 55 s for Rabi spectroscopy and a thermal noise limited instability of 4×10^{-17} .

Description of the experiment

The experimental set-up is presented in Fig. 1. The local oscillator operates at 1,542 nm because Si is not transparent at the Sr clock transition wavelength (698 nm). An optical frequency comb is

¹JILA, National Institute of Standards and Technology and University of Colorado, Department of Physics, University of Colorado, Boulder, CO, USA.

²Physikalisch-Technische Bundesanstalt, Braunschweig, Germany. ³Menlo Systems GmbH, Martinsried, Germany. ⁴Max-Planck-Institut für Quantenoptik, Garching, Germany. ⁵Present address: Department of Molecular and Cellular Physiology, Stanford University, Stanford, CA, USA. ⁶Present address: Horia Hulubei National Institute of Physics and Nuclear Engineering, Magurele, Romania. *e-mail: ericoelker@gmail.com; Ye@jila.colorado.edu

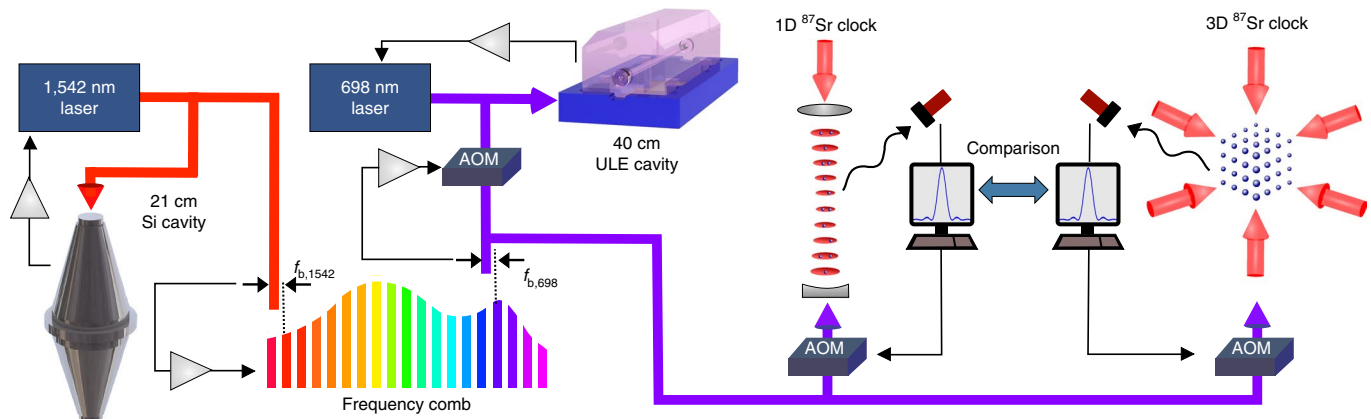


Fig. 1 | Experimental layout. A 1,542 nm laser is stabilized to a 21 cm cryogenic silicon resonator at 124 K using the Pound-Drever-Hall (PDH) technique. The stability is transferred to a self-referenced femtosecond Er-fibre frequency comb that is phase-locked to the 1,542 nm light by actuating on the comb repetition rate. Light from the comb at 1,396 nm is frequency-doubled to the clock transition frequency at 698 nm and used to phase-lock a prestabilized 698 nm laser to complete the stability transfer process. The 698 nm light is then sent to both the 1D and 3D optical lattice clocks over optical links with active path length stabilization. Rabi spectroscopy of the clock transition is performed and frequency offsets between the laser and atomic resonance are detected by measuring the ensemble excited-state fraction via atomic fluorescence using a photomultiplier tube. Two independent digital servos steer the laser frequency using AOMs to lock both probe paths to the corresponding atomic transition. The frequency records for the two clocks are analysed to perform intercomparison measurements.

utilized to transfer the stability of the ultrastable laser at 1,542 nm to 698 nm (see Methods). A prestabilized laser at 698 nm is phase-locked to the comb to complete the stability transfer process. Local oscillator light is then delivered to both a one-dimensional (1D) and 3D ^{87}Sr optical lattice clock via phase-stabilized optical links. For both clocks, an ensemble of ^{87}Sr atoms are first cooled with a magneto-optical trap (MOT) on the 32 MHz wide $^1\text{S}_0 \rightarrow ^1\text{P}_1$ transition at 461 nm. A second narrow-line MOT stage utilizing the 7.6 kHz wide $^1\text{S}_0 \rightarrow ^3\text{P}_1$ intercombination transition at 689 nm cools the atoms to a few microkelvin.

For the 1D clock, the atoms are loaded into a 1D magic-wavelength (813.4 nm) optical lattice with a depth of $180E_r$, where E_r is the lattice photon recoil energy, and spin-polarized by optically pumping into one of the $|^1\text{S}_0, m_F = \pm \frac{9}{2}\rangle$ stretched states. The lattice depth is ramped down to $32E_r$, resulting in atom numbers of 1,500–2,000 and sample temperatures below 1 μK . A 500 mG (1 G = 10^{-4} T) bias field is applied to resolve the Zeeman sublevels and Rabi spectroscopy is first performed on the $|^1\text{S}_0, -\frac{9}{2}\rangle \rightarrow |^3\text{P}_0, -\frac{9}{2}\rangle$ transition. The excited-state population fraction is measured on one side of resonance and then the clock laser frequency is stepped across resonance by one full-width at half-maximum (FWHM) and the population fraction is measured again. The difference between these two excitation fractions yields an error signal proportional to the offset of the clock laser frequency from resonance. This offset is nulled using a digital servo to adjust the laser frequency to remain on resonance using an acousto-optic modulator (AOM). This operation is interleaved with an identical locking scheme for the $|^1\text{S}_0, +\frac{9}{2}\rangle \rightarrow |^3\text{P}_0, +\frac{9}{2}\rangle$ transition. Because the two transitions have opposing first-order Zeeman shifts, the correction signals for the two servos are averaged for all clock stability computations to reject frequency shifts due to fluctuations in the background magnetic field. This technique is effective at rejecting slowly varying field noise but provides almost no rejection of fluctuations at Fourier frequencies above 50 mHz (see Supplementary Information). High-frequency magnetic field fluctuations in the 1D system are typically below the 100 μG level and only modestly impact the clock stability at short averaging times.

For the 3D clock, the atoms are transferred from the 689 nm MOT into a co-located crossed optical dipole trap at 1,064 nm. A trap depth of 1 μK is chosen to remove atoms above the recoil temperature (200 nK). To minimize dead time in this work we elect to forego the evaporative cooling stage used previously²². Approximately 20,000 atoms are then loaded into a 3D magic-wavelength lattice with a depth of $60E_r$ in each direction. To further reduce short-term instability in the 3D system, clock spectroscopy is performed on the $|^1\text{S}_0, \pm \frac{5}{2}\rangle \rightarrow |^3\text{P}_0, \pm \frac{3}{2}\rangle$ transitions, which are 22 times less sensitive to magnetic field noise³², as depicted in Fig. 3. A 1 G bias field is applied followed by a π pulse on the $|^1\text{S}_0, \pm \frac{5}{2}\rangle \rightarrow |^3\text{P}_0, \pm \frac{3}{2}\rangle$ transition. A 5 ms pulse of 461 nm light removes all remaining ground-state atoms, yielding a sample in the $|^3\text{P}_0, \pm \frac{3}{2}\rangle$ excited state with 1,000 ($m_F = -\frac{3}{2}$) or 2,000 ($m_F = +\frac{3}{2}$) atoms. Rabi spectroscopy is then performed from the excited state and the clock laser is stabilized to both the $|^1\text{S}_0, \pm \frac{5}{2}\rangle \rightarrow |^3\text{P}_0, \pm \frac{3}{2}\rangle$ transitions using a four-point locking sequence similar to the 1D system.

The frequency record for both clocks is logged and used to determine the clock stability by computing an Allan deviation of the relative fractional frequency fluctuations (see Methods). All results are reported in terms of the single-clock stability: $\frac{1}{\sqrt{2}}(\nu_{1\text{D}}(t) - \nu_{3\text{D}}(t))/\nu_c$.

Sources of clock instability

To compute an estimate of the Dick effect contribution to the instability of the clocks it is necessary to have a frequency-domain noise model of the local oscillator. Figure 2a depicts a cross-correlation measurement³³ using heterodyne beat signals between the clock laser and two reference ultrastable laser systems. The reference systems are based on a 6 cm Si cavity operating at 4 K (refs. ^{30,31}) and a room-temperature 40 cm ULE cavity²⁶ with thermal noise floors of 6.5×10^{-17} and 8.8×10^{-17} , respectively. From this measurement, we compute the clock instability arising from the Dick effect as^{34,35}

$$\sigma_{\text{Dick}}^2(\tau) = \frac{1}{\tau} \sum_{n=1}^{\infty} \left| \frac{G(n/T_c)}{G(0)} \right|^2 S_y(n/T_c) \quad (2)$$

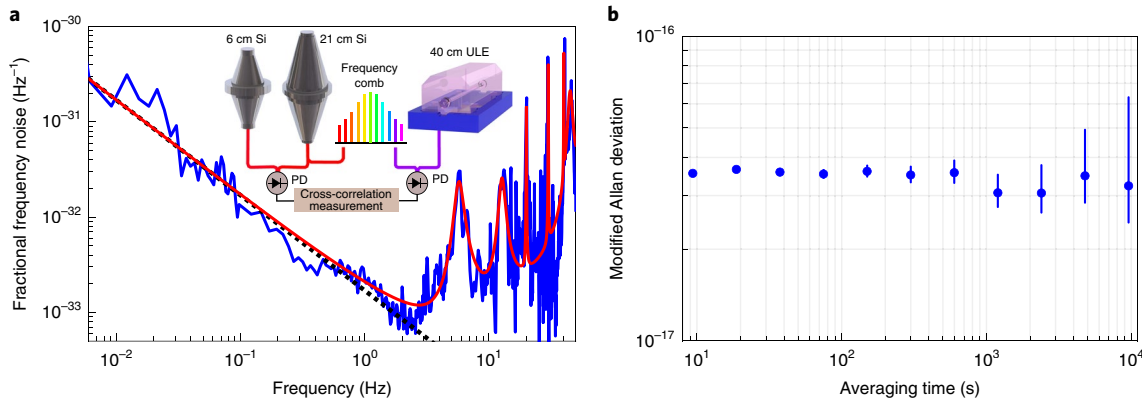


Fig. 2 | Laser stability characterization. **a**, The short-term stability of the 21 cm Si cavity is evaluated by measuring against two reference ultrastable lasers and computing a cross-correlation. Blue trace, cross-spectral density (CSD) of the two signals after 10 h of averaging. Provided that the three systems are uncorrelated, the noise from the reference systems will average away in the CSD, yielding a frequency noise spectrum for the clock laser. The resulting spectrum is consistent with the thermal noise floor (dashed black line) below 3 Hz. A noise model based on this measurement (red trace) is used to predict the Dick-effect-limited stability of both clocks. **b**, Allan deviation of the frequency corrections applied by the atomic servo to stabilize the laser to the clock transition of the 1D lattice clock. This constitutes a direct measurement of the clock laser stability at averaging times where the atomic servo is engaged (>30 s). This 11 h measurement showcases the improved long-term stability of the local oscillator, which now maintains thermal-noise-limited performance at averaging times exceeding 1,000 s. A linear drift rate of $48 \mu\text{Hz s}^{-1}$ at 1,542 nm was subtracted from the frequency record before computing the stability. Error bars indicate 1σ confidence intervals.

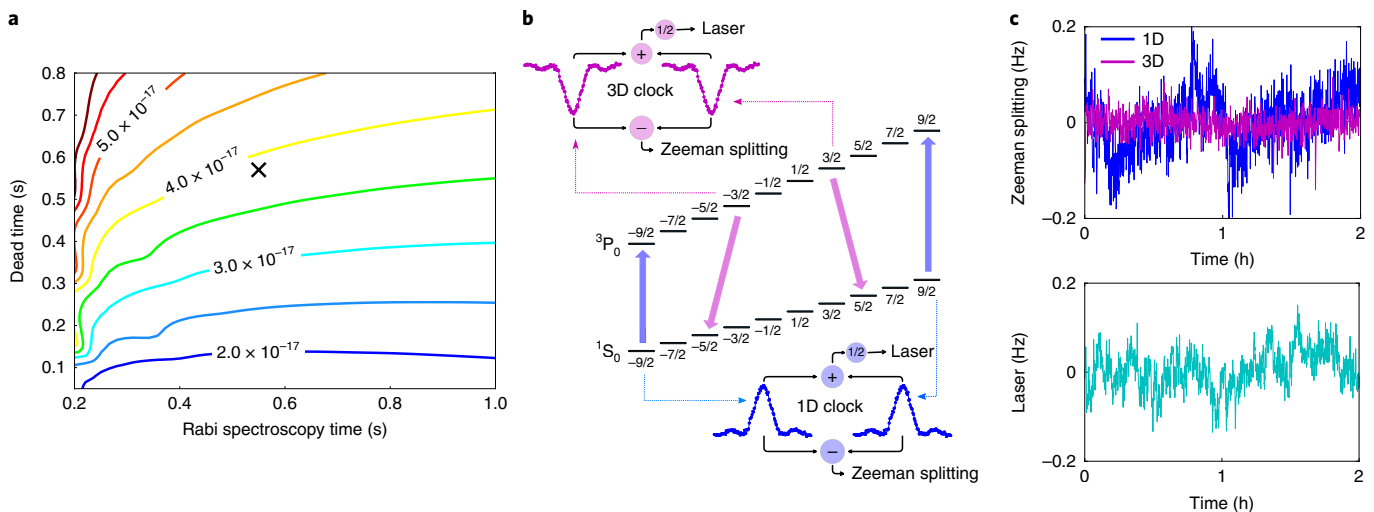


Fig. 3 | Impact of laser and magnetic field noise on clock instability. **a**, Calculation of the Dick-effect-limited instability of an optical clock using Rabi spectroscopy assuming the laser noise model presented in Fig. 2a. The contours show the instability at 1 s as a function of Rabi spectroscopy time and dead time and the marker indicates the operating conditions used for the comparison measurement in Fig. 5a. **b**, Clock spectroscopy for magnetic field noise cancellation. Both systems reject magnetic field noise by alternately interrogating clock transitions in the hyperfine manifold with opposing Zeeman shifts and averaging the measured frequencies before computing the clock stability. This technique is effective for cancelling noise from slow drift in the background field but does little to reject rapid fluctuations. If these unsuppressed fluctuations are comparable to laser noise, they can degrade the clock stability. The 1D clock utilizes π transitions between the stretched states $|\ ^1\text{S}_0, m_F = \pm \frac{9}{2} \rangle \rightarrow |\ ^3\text{P}_0, m_F = \pm \frac{9}{2} \rangle$ with a field sensitivity of 975 Hz G^{-1} . To reject noise from field transients the 3D clock interrogates the $|\ ^1\text{S}_0, m_F = \pm \frac{5}{2} \rangle \rightarrow |\ ^3\text{P}_0, m_F = \pm \frac{3}{2} \rangle_{\sigma_{\pm}}$ transitions, which are split by only 44 Hz G^{-1} . **c**, Fluctuations in the first-order Zeeman splitting between the two interrogated clock transitions are plotted for both systems. A plot of local oscillator frequency fluctuations computed by averaging the stretched state transition frequencies in the 1D clock is included for comparison.

where $S_y(f)$ is the power spectral density of fractional frequency fluctuations of the local oscillator (red trace, Fig. 2a) and $G(f)$ denotes the atomic sensitivity function at Fourier frequency f (see Methods). Figure 3a shows the result of this computation as a function of Rabi interrogation time and dead time. For the operating conditions used in Fig. 5a, we anticipate a Dick effect limit of $3.8 \times 10^{-17} / \sqrt{\tau}$ and a

QPN contribution of $2.9 \times 10^{-17} / \sqrt{\tau}$, yielding a clock instability of $4.8 \times 10^{-17} / \sqrt{\tau}$.

Attaining the best clock stability requires that the local oscillator be converted from 1,542 nm to 698 nm and then distributed to both clocks with minimal loss of phase coherence. Figure 4 depicts a characterization measurement of the optical frequency comb in Fig. 1,

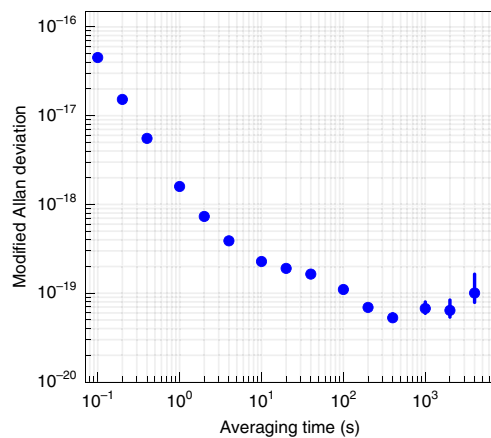


Fig. 4 | Spectral purity transfer of the local oscillator. The noise added to the local oscillator by the frequency comb stability transfer process depicted in Fig. 1 is estimated by performing a multi-line comb comparison with an identical reference system. Both frequency combs are locked to a common reference at 1,542 nm and the beat between their outputs at 698 nm is analysed. The instability of this signal is 1.6×10^{-18} at 1 s. Error bars indicate 1σ confidence intervals.

which demonstrates spectral purity transfer at the 1.6×10^{-18} level at 1 s (see Methods and Supplementary Information). Consequently, the frequency comb is not a significant source of instability.

With such a low instability at 1 s, the clocks reach a precision where drifting systematic offsets that impact the clock performance can be easily identified after only a few hundred seconds of averaging. Active temperature stabilization is implemented on both systems to mitigate fluctuations in Stark shifts arising from blackbody radiation. Variations in the lattice a.c. Stark shift are minimized by stabilizing the lattice intensity and referencing its frequency to the local oscillator using an 813.4 nm output of the optical frequency comb in Fig. 1. The 1D clock is operated with a shallow lattice depth and low atom number to achieve a density shift below 1×10^{-17} ensuring that atom number fluctuations do not impact its stability. This approach allows both clocks to average into the 10^{-19} decade, without requiring frequency corrections to compensate for non-stationary systematics.

Clock instability measurements

The instability of the two systems is evaluated by performing both an anti-synchronous comparison where clock spectroscopy for the two systems has no temporal overlap and a synchronous comparison where clock spectroscopy is performed simultaneously. We do not report the frequency offset between the two systems based on these measurements, as only the 1D lattice clock has undergone a full evaluation of its systematic offsets³⁶. An anti-synchronous comparison is sensitive to all sources of instability including the Dick effect, QPN, fluctuating systematic offsets and other sources of technical noise, and it provides an estimate of the performance both clocks achieve individually. Both clocks operate with a spectroscopy time of 550 ms and a dead time of 570 ms, where the two clock interrogations are offset from one another to ensure no overlap. When operating in this configuration with a shared local oscillator,

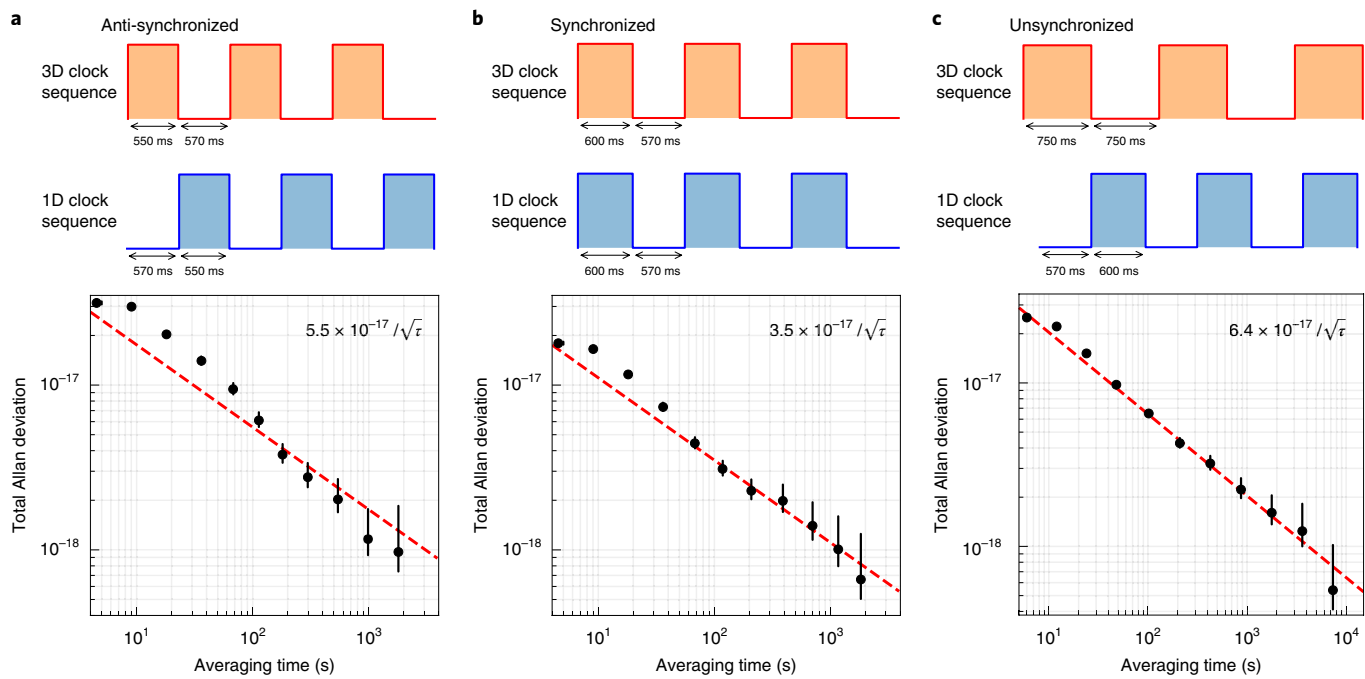


Fig. 5 | Stability comparison between 1D and 3D clocks. The total Allan deviation of the fractional measurement instability is reported as $\frac{1}{\sqrt{2}}(\nu_{1D}(t) - \nu_{3D}(t))\nu_c$. Dashed red lines represent a weighted $1/\sqrt{t}$ fit to the data past 80 s and extend out to the full measurement time for each comparison. **a**, Anti-synchronous comparison. The two clocks are run with the clock pulses anti-synchronized to prevent common mode rejection of the Dick effect. The observed instability of $5.5(3) \times 10^{-17}/\sqrt{t}$ along with a detailed noise model allow one to infer an instability of $4.8 \times 10^{-17}/\sqrt{t}$ for independent clock operation. **b**, Synchronous comparison. The two clock pulses are synchronized to provide maximal common mode rejection of the Dick effect. An instability of $3.5(2) \times 10^{-17}/\sqrt{t}$, limited primarily by QPN, is observed. The final data point at 1,800 s reaches a value of 6.6×10^{-19} . **c**, Unsynchronized comparison. This measurement demonstrates the capability of both clocks to average down with state-of-the-art stability for a comparison spanning several hours. An instability of $6.4(1) \times 10^{-17}/\sqrt{t}$ is observed. Error bars indicate 1σ confidence intervals.

the added noise from the Dick effect in the two systems exhibits some anti-correlation and the measured instability is expected to be higher than the prediction from equation (2) (see Methods). As shown in Fig. 5a, this measurement attains an instability of $5.5(3) \times 10^{-17}/\sqrt{\tau}$, in excellent agreement with the anticipated limit of $5.7 \times 10^{-17}/\sqrt{\tau}$ from QPN and the Dick effect. From this measurement and the noise model, one can deduce a single-clock instability of $4.8 \times 10^{-17}/\sqrt{\tau}$ for independent operation (that is, when compared with an uncorrelated reference). This is a threefold improvement over previously reported values^{1,4,19–21} and a nearly 10-fold reduction in the corresponding averaging time.

Synchronous interrogation^{4,6,19,20,37,38} can further improve stability through common-mode rejection of the Dick effect. In principle, this can facilitate comparison measurements limited solely by QPN, although this requires disseminating the local oscillator to all atomic ensembles under interrogation with exceptionally high fidelity. Synchronous interrogation has led to stability improvements for clock comparisons within a single laboratory^{4,19,20,37,38} or over a regional fibre network⁶, but is less practical over the longer distances envisaged for a future global network of optical clocks³⁹. Figure 5b depicts a synchronous comparison where both clocks operate with 600 ms spectroscopy time and 570 ms dead time. An instability of $3.5(2) \times 10^{-17}/\sqrt{\tau}$ is observed, near the expected QPN limit of $2.9 \times 10^{-17}/\sqrt{\tau}$. Each clock averages to a value of 6.6×10^{-19} , as determined by the final Allan deviation point at 1,800 s.

A third dataset, taken before optimizing the dead time of the 3D clock, is presented in Fig. 5c. This unsynchronized comparison has a different sensitivity to the Dick effect than the anti-synchronous comparison and provides an additional validation of the noise model (see Methods). The clocks average at a rate of $6.4(1) \times 10^{-17}/\sqrt{\tau}$. The final data point at 7,400 s corresponds to a stability of 5.4×10^{-19} .

Discussion

The results presented here represent a significant advance in optical clock stability. An almost order-of-magnitude decrease in measurement time will accelerate the development of clocks with 10^{-19} level accuracy. Future work will focus on improving the local oscillator both to reduce the Dick effect and to lower the QPN limit by extending the clock interrogation time. Combining cryogenic silicon cavities with AlGaAs optical coatings⁴⁰ provides a path towards laser stabilization at the low 10^{-18} level^{29,30} and laser coherence times approaching the natural lifetime of the clock excited state (~ 150 s for ^{87}Sr). Fully utilizing such a laser will require new techniques to improve the atomic coherence time⁴¹, which, so far⁴², has been limited to < 10 s. With further advances in laser and atomic coherence, clock stability can be improved by another order of magnitude or more.

Online content

Any methods, additional references, Nature Research reporting summaries, source data, statements of code and data availability and associated accession codes are available at <https://doi.org/10.1038/s41566-019-0493-4>.

Received: 6 February 2019; Accepted: 19 June 2019;

Published online: 29 July 2019

References

- Bloom, B. J. et al. An optical lattice clock with accuracy and stability at the 10^{-18} level. *Nature* **506**, 71–75 (2014).
- Nicholson, T. L. et al. Systematic evaluation of an atomic clock at 2×10^{-18} total uncertainty. *Nat. Commun.* **6**, 6896 (2015).
- Huntemann, N., Sanner, C., Lipphardt, B., Tamm, C. & Peik, E. Single-ion atomic clock with 3×10^{-18} systematic uncertainty. *Phys. Rev. Lett.* **116**, 063001 (2016).
- McGrew, W. F. et al. Atomic clock performance enabling geodesy below the centimetre level. *Nature* **564**, 87–90 (2018).
- Brewer, S. M. et al. $^{27}\text{Al}^+$ quantum-logic clock with a systematic uncertainty below 10^{-18} . *Phys. Rev. Lett.* **123**, 033201 (2019).
- Takano, T. et al. Geopotential measurements with synchronously linked optical lattice clocks. *Nat. Photon.* **10**, 662–666 (2016).
- Riehle, F. Towards a redefinition of the second based on optical atomic clocks. *C. R. Phys.* **16**, 506–515 (2015).
- Huntemann, N. et al. Improved limit on a temporal variation of m_p/m_e from comparisons of Yb^+ and Cs atomic clocks. *Phys. Rev. Lett.* **113**, 210802 (2014).
- Godun, R. M. et al. Frequency ratio of two optical clock transitions in $^{171}\text{Yb}^+$ and constraints on the time variation of fundamental constants. *Phys. Rev. Lett.* **113**, 210801 (2014).
- Rosenband, T. et al. Frequency ratio of Al^+ and Hg^+ single-ion optical clocks; metrology at the 17th decimal place. *Science* **319**, 1808–1812 (2008).
- Chou, C. W., Hume, D. B., Rosenband, T. & Wineland, D. J. Optical clocks and relativity. *Science* **329**, 1630–1633 (2010).
- Grotti, J. et al. Geodesy and metrology with a transportable optical clock. *Nat. Phys.* **14**, 437–441 (2018).
- Sanner, C. et al. Optical clock comparison test of Lorentz symmetry. *Nature* **567**, 204–208 (2019).
- Delva, P. et al. Test of special relativity using a fiber network of optical clocks. *Phys. Rev. Lett.* **118**, 221102 (2017).
- Kolkowitz, S. et al. Gravitational wave detection with optical lattice atomic clocks. *Phys. Rev. D* **94**, 124043 (2016).
- Derevianko, A. & Pospelov, M. Hunting for topological dark matter with atomic clocks. *Nat. Phys.* **10**, 933–936 (2014).
- Arvanitaki, A., Huang, J. & Van Tilburg, K. Searching for dilaton dark matter with atomic clocks. *Phys. Rev. D* **91**, 015015 (2015).
- Itano, W. M. et al. Quantum projection noise: population fluctuations in two-level systems. *Phys. Rev. A* **47**, 3554–3570 (1993).
- Schioppo, M. et al. Ultra-stable optical clock with two cold-atom ensembles. *Nat. Photon.* **11**, 48–52 (2017).
- Nicholson, T. L. et al. Comparison of two independent Sr optical clocks with 1×10^{-17} stability at 10^3 s. *Phys. Rev. Lett.* **109**, 230801 (2012).
- Al-Masoudi, A., Dörscher, S., Häfner, S., Sterr, U. & Lisdat, C. Noise and instability of an optical lattice clock. *Phys. Rev. A* **92**, 063814 (2015).
- Campbell, S. L. et al. A Fermi-degenerate three-dimensional optical lattice clock. *Science* **358**, 90–94 (2017).
- Kolkowitz, S. et al. Spin-orbit-coupled fermions in an optical lattice clock. *Nature* **542**, 66–70 (2017).
- Zhang, X. et al. Spectroscopic observation of SU(N)-symmetric interactions in Sr orbital magnetism. *Science* **345**, 1467–1473 (2014).
- Martin, M. J. et al. A quantum many-body spin system in an optical lattice clock. *Science* **341**, 632–636 (2013).
- Bishof, M., Zhang, X., Martin, M. J. & Ye, J. Optical spectrum analyzer with quantum-limited noise floor. *Phys. Rev. Lett.* **111**, 093604 (2013).
- Häfner, S. et al. 8×10^{-17} fractional laser frequency instability with a long room-temperature cavity. *Opt. Lett.* **40**, 2112–2115 (2015).
- Kessler, T. et al. A sub-40-mHz-linewidth laser based on a silicon single-crystal optical cavity. *Nat. Photon.* **6**, 687–692 (2012).
- Matei, D. G. et al. 1.5 μm lasers with sub-10 mHz linewidth. *Phys. Rev. Lett.* **118**, 263202 (2017).
- Zhang, W. et al. Ultrastable silicon cavity in a continuously operating closed-cycle cryostat at 4 K. *Phys. Rev. Lett.* **119**, 243601 (2017).
- Robinson, J. M. et al. Crystalline optical cavity at 4 K with thermal noise limited instability and ultralow drift. *Optica* **6**, 240–243 (2019).
- Boyd, M. M. et al. Nuclear spin effects in optical lattice clocks. *Phys. Rev. A* **76**, 022510 (2007).
- Rubiola, E. & Vernotte, F. The cross-spectrum experimental method. Preprint at <https://arxiv.org/abs/1003.0113> (2010).
- Dick, J. G. Local oscillator induced instabilities in trapped ion frequency standards. In *Proceedings of the 19th Annual Precise Time and Time Interval Meeting*, 133–147 (US Naval Observatory, 1988); https://tycho.usno.navy.mil/ptti/1987papers/Vol%202019_13.pdf
- Santarelli, G. et al. Frequency stability degradation of an oscillator slaved to a periodically interrogated atomic resonator. *IEEE Trans. Ultrason. Ferroelectr. Freq. Control* **45**, 887 (1998).
- Bothwell, T. et al. JILA Sr1 optical lattice clock with uncertainty of 2.0×10^{-18} . Preprint at <https://arxiv.org/abs/1906.06004> (2019).
- Takamoto, M., Takano, T. & Katori, H. Frequency comparison of optical lattice clocks beyond the Dick limit. *Nat. Photon.* **5**, 288–292 (2011).
- Ushijima, I., Takamoto, M., Das, M., Ohkubo, T. & Katori, H. Cryogenic optical lattice clocks. *Nat. Photon.* **9**, 185–189 (2015).
- Riehle, F. Optical clock networks. *Nat. Photon.* **11**, 25–31 (2017).
- Cole, G. D., Zhang, W., Martin, M. J., Ye, J. & Aspelmeyer, M. Tenfold reduction of Brownian noise in high-reflectivity optical coatings. *Nat. Photon.* **7**, 644–650 (2013).

41. Hutson, R. B., Goban, A., Marti, G. E. & Ye, J. Engineering quantum states of matter for atomic clocks in shallow optical lattices. Preprint at <https://arxiv.org/abs/1903.02498> (2019).
42. Marti, G. E. et al. Imaging optical frequencies with 100 µHz precision and 1.1 µm resolution. *Phys. Rev. Lett.* **120**, 103201 (2018).

Acknowledgements

This work is supported by the National Institute of Standards and Technology (NIST), the Defense Advanced Research Projects Agency (DARPA), the Air Force Office of Scientific Research Multidisciplinary University Research Initiative, the National Science Foundation (NSF) JILA Physics Frontier Center (NSF PHY-1734006), the Cluster of Excellence (EXC 2132 Quantum Frontiers) and Physikalisch-Technische Bundesanstalt (PTB). E.O. and C.J.K. are supported by a postdoctoral fellowship from the National Research Council. L.S. is supported by a National Defense Science and Engineering Graduate Fellowship. A.G. is supported by a fellowship from the Japan Society for the Promotion of Science and C.S. is supported by a fellowship from the Humboldt Foundation. T.L., D.G.M. and U.S. acknowledge support from the Quantum sensors (Q-SENSE) project, supported by the European Commission's H2020 Marie Skłodowska-Curie Actions Research and Innovation Staff Exchange (MSCA RISE) under grant agreement no. 69115. M.G. and R.H. acknowledge support from the EU FP7 initial training network FACT (Future Atomic Clock Technology) and the DARPA Program in Ultrafast Laser Science and Engineering (PureComb project) under contract no.

W31P4Q-14-C-0050. The authors thank J. Munez and J. Sherman for careful reading of this manuscript.

Author contributions

E.O., R.B.H., C.J.K., T.B., L.S., C.S., D.K., A.G., J.M.R., G.E.M. and J.Y. contributed to the clock instability measurements. E.O., J.M.R., L.S., C.J.K., T.B., D.K., D.G.M., T.L., F.R., U.S. and J.Y. worked on the Si cavity. L.S. and E.O. commissioned the laser stability transfer set-up based on the Er frequency comb developed by M.G. and R.H. All authors contributed to scientific discussions and the writing of this manuscript.

Competing interests

The authors declare no competing interests.

Additional information

Supplementary information is available for this paper at <https://doi.org/10.1038/s41566-019-0493-4>.

Reprints and permissions information is available at www.nature.com/reprints.

Correspondence and requests for materials should be addressed to E.O. or J.Y.

Publisher's note: Springer Nature remains neutral with regard to jurisdictional claims in published maps and institutional affiliations.

© The Author(s), under exclusive licence to Springer Nature Limited 2019

Methods

Optical local oscillator. A distributed feedback fibre laser operating at 1,542 nm is stabilized to a 21 cm single-crystal silicon cavity with a finesse of 480,000 using the PDH technique. The cavity is actively temperature-stabilized to 124 K where the coefficient of thermal expansion for silicon goes to zero. The temperature actuation is realized with a custom low-vibration cryostat using evaporated liquid nitrogen²⁸. The cavity is mounted vertically near the midplane using a three-point support structure to minimize the impact of vibrations on its length stability. The cavity chamber is maintained at a pressure of 10^{-10} mbar and located on an active vibration isolation platform. Active residual amplitude modulation (RAM) control⁴³ and intensity stabilization are implemented to optimize the long-term stability.

The performance of the local oscillator, referred to as Silicon 3 in previous publications, was reported in ref. ²⁹. This system was recently relocated to JILA and a new characterization of its performance was necessary due to the change in operating environment. By direct evaluation with a Sr clock and through extensive three-cornered-hat measurements against two reference ultrastable lasers^{26,30}, the cavity instability was typically observed to be thermal-noise-limited at a level of 3.7×10^{-17} between 0.2 and 1,000 s, although thermal noise performance occasionally extends to longer averaging times (Fig. 2b and Supplementary Fig. 6). The improved long-term stability of the local oscillator is described in ref. ⁴⁴.

A frequency-domain laser noise model based on a cross-correlation measurement³³ is used to estimate the Dick-effect-limited instability of both clocks. The cross-spectral density of the heterodyne beats between our local oscillator and two reference ultrastable lasers^{26,30} is presented in Fig. 2a. Provided that the three systems are uncorrelated, the noise from the two reference systems will average away, yielding an estimate of the power spectral density of the local oscillator's fractional frequency noise. The resulting noise spectrum is used to construct the following model:

$$S_{\text{laser}}(f) = \frac{h_{-1}}{f} + h_0 + f^2 h_2 + \sum_{i=1}^N \frac{a f^2}{1 + \left(\frac{f - f_i}{T_i/2}\right)^2} \quad (3)$$

This model consists of a flicker frequency noise term ($h_{-1} = 1.5 \times 10^{-33}$), a white frequency noise term ($h_0 = 4 \times 10^{-34} \text{ Hz}^{-1}$), a white phase noise term ($h_2 = 3 \times 10^{-36} \text{ Hz}^{-3}$) and a series of resonant features (parameters given in Supplementary Table 1). The model differs from that reported in ref. ²⁹, because of a slightly lower seismic noise background at JILA.

Spectral purity transfer of the local oscillator. The stability of the local oscillator is transferred from 1,542 nm to the clock transition wavelength at 698 nm using an ultralow-noise optical frequency comb. The comb is based on a femtosecond Er-doped polarization-maintaining fibre oscillator⁴⁵ operating at a repetition rate (f_{rep}) of 250 MHz and a centre wavelength of 1,560 nm. The oscillator contains two intra-cavity electro-optic modulators that enable MHz bandwidth stabilization of both f_{rep} and the carrier-envelope offset frequency (f_{cko}) with minimal crosstalk⁴⁶. Additional low-bandwidth piezo and thermal actuators extend the tuning range of f_{rep} enabling the comb to remain locked for months at a time.

The output of the femtosecond laser is amplified and split to seed two distinct comb branches. The first arm generates an octave-spanning spectrum used to measure f_{cko} via an f - $2f$ interferometer. The second branch is designed to achieve low-noise spectral purity transfer by providing outputs at both 1,542 nm and 698 nm with minimal differential path length fluctuations. A narrowband spectrum at 1,397 nm is generated using four-wave mixing in a highly nonlinear fibre. A portion of the transmitted seed light is picked off to form a heterodyne beat with the local oscillator. As depicted in Fig. 1, this signal is used to phase-lock the comb to the local oscillator by actuating on f_{rep} . The second output of this branch is frequency-doubled using a periodically poled lithium niobate crystal to produce a 2.5 nm FWHM spectrum centred at 698.4 nm. A pre-stabilized external-cavity diode laser is then phase-locked to the 698 nm comb output with a bandwidth of 1 kHz to complete the transfer process.

The fidelity of the stability transfer is assessed by performing a multi-line comb comparison with an identical reference system to characterize the differential noise between the 1,542 nm and 698 nm outputs⁴⁷. A well defined comb line for each system is phase-locked to a common optical reference at 1,542.14 nm. The lock points for the f_{cko} and f_{rep} stabilization servos are chosen such that the combs operate with the same repetition rate and their spectral lines are offset from one another by 5 MHz across the near-infrared optical domain. A heterodyne beat at 10 MHz is formed between the frequency-doubled outputs of the two combs at 698 nm and counted using a dead-time free lambda-type frequency counter with a 100 ms gate time. Based on this qualification, both combs perform the transfer from 1,542 nm to 698 nm with a fractional instability of 1.6×10^{-18} at 1 s and any degradation in the stability of the clock laser is expected to be negligible (Fig. 4 and Supplementary Fig. 7).

Optical path length stabilization. To eliminate first-order Doppler shifts when performing spectroscopy on the clock transition, the optical paths depicted in Fig. 1 between the frequency comb and the retro-reflector for the optical lattice in

each clock are actively stabilized using standard techniques⁴⁸. These optical paths are operated in a pulsed fashion because the clock light must be extinguished during the dead time interval between successive clock measurements. Such pulsed operation is a known source of phase transients arising from the finite settling time of the path length stabilization servo⁴⁹. To remove the impact of this effect on the clock stability, the lock point of the path length stabilization servo is offset to detune the clock light from resonance by 1 MHz before re-engaging the servo. After waiting an appropriate interval to allow any phase transients to decay, the laser frequency is swept continuously over a 3 ms interval to the desired value for clock spectroscopy. This frequency ramp produces no appreciable ringing in the path length stabilization servo. Systematic offsets arising from this method have not been studied experimentally so far, although our theoretical calculation indicates that offsets arising from off-resonant excitation during the frequency ramp should be below the 2×10^{-19} level.

Clock spectroscopy time. The performance of the local oscillator used in this work allows for clock interrogation times exceeding 10 s (ref. ²⁹). However, density-dependent effects in the 1D lattice clock result in lineshape distortion and loss of contrast for spectroscopy times exceeding 1 s (ref. ²⁵). For this reason, a more conservative spectroscopy time of 600 ms is used. The use of a 3D lattice²² or a 1D lattice with a larger mode volume^{1,2} can significantly reduce these effects in future experiments.

Atomic sensitivity function. The Dick effect^{34,35} is a source of instability in optical clocks arising from the aliasing of laser noise at integer multiples of the clock cycle frequency (n/T_c where n is an integer) down to d.c. It sets a bound on the achievable fractional frequency instability of a single clock given by equation (2). $G(f)$ in equation (2) is the Fourier transform of the atomic sensitivity function $g(t) = 2 \frac{\delta p_e}{\delta \phi}$, which describes the change induced in the excitation fraction (δp_e) by a phase shift in the local oscillator ($\delta \phi$) at time t . For Rabi spectroscopy beginning at time $t=0$, the sensitivity function is given by³⁴

$$\begin{aligned} g(t) &= \sin^2(\theta) \cos(\theta) \\ &\times [\sin(\Omega_1(t)) (1 - \cos(\Omega_2(t))) + \sin(\Omega_2(t)) \\ &\quad (1 - \cos(\Omega_1(t)))] , \quad 0 \leq t \leq T_p \\ &= 0, \quad T_p < t \leq T_c \end{aligned} \quad (4)$$

with $\theta = \pi/2 - \arctan(2\Delta T_p)$, where $\Delta \approx \frac{0.4}{T_p}$ is the detuning from resonance for clock spectroscopy, $\Omega_1(t) = \pi \sqrt{1 + (2\Delta T_p)} \frac{t}{T_p}$ and $\Omega_2(t) = \pi \sqrt{1 + (2\Delta T_p)} \frac{T_p - t}{T_p}$.

Clock instability measurements. To determine the instability of the 1D and 3D clocks, we measure the relative fractional frequency fluctuations between the systems. Assuming that the two clocks have identical noise levels but are uncorrelated, the single clock instability can be inferred by analysing

$$\frac{1}{\sqrt{2}} \frac{\nu_{1D}(t) - \nu_{3D}(t)}{\nu_c} \quad (5)$$

where $\nu_{1D}(t)$ is the frequency record for the 1D clock, $\nu_{3D}(t)$ is the frequency record for the 3D clock and ν_c is the Sr clock transition frequency. For the unsynchronized comparison in Fig. 5c, the frequency record of the 1D clock is interpolated to match the measurement times of the 3D clock before computing the instability.

In similar comparison measurements^{1,4,19,20}, the frequency record of each clock is typically derived from the frequency corrections applied by the clock servo to keep the laser on resonance. However the atomic servos have a finite bandwidth (30 mHz), and short-term fluctuations between the laser frequency and the atomic resonance are not fully accounted for in the correction signal. One can gain additional information about the noise present at higher Fourier frequencies by also examining the servo error signal. In this Article, the error signal is used to correct the frequency record for each servo as follows⁵²

$$\nu(t_i) = \nu_{\text{corr}}(t_{i-1}) + \frac{\Gamma}{2A} \times \delta p_e(t_i) \quad (6)$$

where t_i is the measurement time for the i th clock cycle, $\nu_{\text{corr}}(t_{i-1})$ is the servo correction signal, Γ is the FWHM linewidth, A is the excitation fraction at the peak of the atomic resonance and $\delta p_e(t_i)$ is the error signal given by the difference between the measured excitation fraction on the left and right side of resonance. After correcting for the error signal, the Allan deviation for a measurement limited solely by QPN and the Dick effect is expected to follow a constant $1/\sqrt{\tau}$ slope at all averaging times. The fact that the traces in Fig. 5 deviate from this behaviour at short averaging times indicates the presence of additional short-term noise. In all three comparisons, the noise on the 1D clock exceeds that of the 3D clock at averaging times below 40 s. High-frequency magnetic-field-induced noise is not efficiently rejected by the spectroscopy sequence (see Supplementary Information) and is a plausible cause of excess instability at these averaging times in a clock with this level of precision. Implementing clock spectroscopy on the

$|^1S_0, \pm \frac{5}{2}\rangle \rightarrow |^3P_0, \pm \frac{3}{2}\rangle$ transitions proved impractical in the 1D system due to an insufficient atom number after state preparation.

To give this short-term noise sufficient time to average away, a weighted $1/\sqrt{\tau}$ fit is applied to Allan deviation points beyond 80 s when determining the instability in each comparison measurement. All instability calculations use the total Allan deviation, with error bars computed according to ref. ⁵⁰.

Dick effect prediction. Although the assumption that the noise contributions from the two clocks are uncorrelated is correct for the QPN contributions that dominate the synchronous comparison, it is only approximately true for the anti-synchronized and unsynchronized comparisons because the two clocks share the same local oscillator and correlations remain, even when the clock interrogations have no temporal overlap. To quantify this effect for the anti-synchronized comparison, one can derive an alternative form of equation (2) to compute the Dick effect limit for a comparison between two clocks with sequences that are identical other than a timing offset of Δt . Examining equations (4) and (5), one notes that this scenario is equivalent to a single clock with an effective sensitivity function of $[g(t + \Delta t) - g(t)]/\sqrt{2}$. Using the shift theorem for the discrete Fourier transform, the n th Fourier-transform coefficient of $g(t + \Delta t)$ is given by $G(f_n)e^{2\pi i n \Delta t/T_c}$. One can then modify equation (2) as follows:

$$\begin{aligned} \sigma_{\text{Dick}}^2(\tau) &= \frac{1}{2\tau} \sum_{n=1}^{\infty} |e^{2\pi i n \Delta t/T_c} - 1|^2 \left| \frac{G(n/T_c)}{G(0)} \right|^2 S_y(n/T_c) \\ &= \frac{2}{\tau} \sum_{n=1}^{\infty} \sin^2\left(\frac{\pi n \Delta t}{T_c}\right) \left| \frac{G(n/T_c)}{G(0)} \right|^2 S_y(n/T_c) \end{aligned} \quad (7)$$

For the anti-synchronous comparison ($\Delta t = 560$ ms), the laser noise model predicts a Dick effect limit of $5.0 \times 10^{-17}/\sqrt{\tau}$, 30% higher than the prediction for independent clock operation. The $n=1$ term in equation (7), which dominates the sum, is inflated by sampling noise at a Fourier frequency of $1/T_c$ using two clocks with $\Delta t = T_c/2$. The noise at this Fourier frequency ends up being strongly anti-correlated between the two systems. The anti-synchronous result therefore represents an upper limit for the single clock instability. Adding this in quadrature with QPN yields a prediction of $5.7 \times 10^{-17}/\sqrt{\tau}$, in excellent agreement with the measured instability of $5.5(3) \times 10^{-17}/\sqrt{\tau}$.

For the unsynchronized comparison in Fig. 5c, the 1D and 3D clocks operate with different cycle and Rabi interrogation times and equation (7) does not apply. To estimate the Dick effect, a frequency record for both clocks is computed numerically using simulated laser noise data based on the noise model, and the instability is calculated according to equation (5). This results in an anticipated instability of $6.0 \times 10^{-17}/\sqrt{\tau}$, in reasonable agreement with the measured value.

Data availability

The data that support the findings of this study are available from the corresponding authors upon reasonable request.

References

43. Zhang, W. et al. Reduction of residual amplitude modulation to 1×10^{-6} for frequency modulation and laser stabilization. *Opt. Lett.* **39**, 1980–1983 (2014).
44. Milner, W. R. et al. Demonstration of a time scale based on a stable optical carrier. Preprint at <https://arxiv.org/abs/1907.03184> (2019).
45. Hänsel, W. et al. All polarization-maintaining fiber laser architecture for robust femtosecond pulse generation. *Appl. Phys. B* **123**, 41 (2017).
46. Hänsel, W., Giunta, M., Fischer, M., Lezius, M. & Holzwarth, R. Rapid electro-optic control of the carrier-envelope-offset frequency for ultra-low noise frequency combs. In *Proceedings of the Joint Conference of the European Frequency and Time Forum and IEEE International Frequency Control Symposium* 128–129 (IEEE, 2017).
47. Giunta, M., Hänsel, W., Fischer, M., Lezius, M. & Holzwarth, R. Sub-mHz spectral purity transfer for next generation strontium optical atomic clocks. In *Proceedings of the Conference on Lasers and Electro-Optics SM1L.5* (OSA, 2018).
48. Ma, L. S., Jungner, P., Ye, J. & Hall, J. L. Delivering the same optical frequency at two places: accurate cancellation of phase noise introduced by an optical fiber or other time-varying path. *Opt. Lett.* **19**, 1777–1779 (1994).
49. Falke, S., Misera, M., Sterr, U. & Lisdat, C. Delivering pulsed and phase stable light to atoms of an optical clock. *Appl. Phys. B* **107**, 301–311 (2012).
50. Howe, D. The total deviation approach to long-term characterization of frequency stability. *IEEE Trans. Ultrason. Ferroelectr. Freq. Control* **47**, 1102–1110 (2000).